International Journal of Greenhouse Gas Control 5 (2011) 1002–1015

Contents lists available at ScienceDirect

International Journal of Greenhouse Gas Control

journal homepage: www.elsevier.com/locate/ijggc

On the potential of CO_2–water–rock interactions for CO_2 storage using a modified kinetic model

V.T.H. Pham [a,*], P. Lu [b], P. Aagaard [a], C. Zhu [b], H. Hellevang [a]

[a] Department of Geosciences, University of Oslo, Pb. 1047, Blindern, Oslo, Norway
[b] Department of Geological Sciences, Indiana University, Bloomington, IN 47405, USA

ARTICLE INFO

Article history:
Received 30 June 2010
Received in revised form 22 October 2010
Accepted 14 December 2010
Available online 15 January 2011

Keywords:
CO_2 storage
Mineral trapping
TST
Ankerite
Dawsonite
BCF
Nucleation theory

ABSTRACT

During CO_2 storage, mineral trapping is the safest long-term storage mechanism, and it is therefore important to estimate the correct CO_2 portion trapped in secondary mineral phases. The storage potential for cold, quartz-rich reservoirs, hereafter termed Utsira-type reservoirs, were solved using the numerical code PHREEQC, using a rate model that took into account both nucleation and growth of secondary mineral phases. This represented a modification of earlier simulations where growth rates were calculated from dissolution rate data. Because growth rate and nucleation rate parameters were largely unknown for the secondary carbonates, we did a sensitivity study on the potential for carbonate growth on rate parameters.

The simulations suggest that the total amount of CO_2 trapped as mineral carbonates is given by the amount of glauconite, chlorite, and smectite present in the reservoir prior to injection, as they were nearly completely dissolved. The fast dissolution of the silicates provided divalent cations for the growth of ankerite and siderite. The timing of precipitation and the secondary mineral assemblage were seen to be highly sensitive to the nucleation and growth rates. Moreover, at high nucleation rates, the secondary carbonates started to precipitate at fairly low supersaturations and formed rapidly after the dissolution of the primary minerals.

Finally, a comparison of earlier simulations on the Utsira-type system with the present model and natural analogues, suggests that the earlier models have largely overestimated the growth potential of carbonates such as dolomite, magnesite and dawsonite.

1. Introduction

Underground sequestration of carbon dioxide is a potentially viable greenhouse gas mitigation option by reducing the release rate of CO_2 to the atmosphere (Holloway, 2004; Enting et al., 2008). CO_2 can be trapped in underground reservoirs by four storage mechanisms: (1) structural and stratigraphic trapping; (2) residual CO_2 trapping; (3) solubility trapping; and (4) mineral trapping (Bachu et al., 2007). Mineral trapping has been considered as the safest mechanism in long-term storage of CO_2 (IPCC, 2005).

Information on the potential of mineral carbonation during CO_2 storage is available from natural systems where CO_2 has reacted with the minerals for extended time periods (Flaathen et al., 2009; Gaus et al., 2005; Moore et al., 2005; Pauwels et al., 2007; Worden, 2006), from numerical simulations of a range of systems (e.g., André et al., 2007; Cantucci et al., 2009; Gaus et al., 2005; Johnson et al., 2004, 2005; Knauss et al., 2005; Xu et al., 2004, 2007; Zhang et al., 2009), from field-scale test-sites (Assayag et al., 2009; Raistrick et al., 2009; Gislason et al., 2010), and from laboratory experiments on mineral stabilities (e.g., Hellevang et al., 2005; Ketzer et al., 2009; Pokrovsky et al., 2009; Saldi et al., 2009). Because natural mineral conversion rates are slow relative to laboratory time scales, the best information on the long-term interactions between CO_2 charged waters and minerals are available from natural analogues. The natural analogues, such as the North Sea Jurassic Sleipner West gas condensate field (Ranaweera, 1987) and the Upper Jurassic sandstones of the Magnus field (Baines and Worden, 2004; Macaulay et al., 1993), the Ladbroke in Australia (Watson et al., 2004) and the Montmiral CO_2 accumulation in France (Pauwels et al., 2007), shows that carbonate minerals like dolomite and ankerite typically form.

For reservoirs like the Utsira Sand where CO_2 has been injected since 1996, data are available for the CO_2 plume migration through 3D seismic shot in 1999, 2001, 2002, 2004 and 2006 (Hermanrud et al., 2009), however, there is no direct observations of the mineral alteration after the CO_2 injection. Previous numerical simulations of CO_2 storage in the Utsira Sand or other similar siliciclastic reservoirs suggested that carbonate minerals such as dawsonite,

* Corresponding author.
E-mail address: vtpham@geo.uio.no (V.T.H. Pham).

1750-5836/$ – see front matter © 2010 Elsevier Ltd. All rights reserved.
doi:10.1016/j.ijggc.2010.12.002

dolomite, siderite and magnesite may form (Johnson et al., 2004, 2005; Audigane et al., 2007; Gaus et al., 2005). The uncertainty, however, is large in the amount of the carbonates and on the composition of the carbonate precipitation assemblage that is predicted to form. For some carbonate minerals, like dawsonite and magnesite, the numerical simulations may have overestimated the amounts that forms compared to the what is observed in natural analogues (Haszeldine et al., 2005; Gaus et al., 2008; Hellevang and Aagaard, 2010).

The differences in the outcome of numerical simulations compared to natural observations may be explained by factors like: (1) incorrect assumptions for natural analogues on key factors like timing of CO_2 charged and possible variations in CO_2 pressures with time; (2) errors in thermodynamic and kinetic data for mineral phases used for the numerical simulations; and (3) kinetic expressions for mineral reactions that are too generalized to calculate properly (Gaus et al., 2008). The last issue is explored based on recent experimental work on carbonate reaction rates that suggests that the conventional method of using dissolution rate coefficients and apparent activation energies to predict growth rates may not be correct.

The conventional method of modelling mineral reaction rates assumes that parameters like the reaction rate coefficients and activation energies are constants that are independent of the affinity of the reaction. Using the transition-state-theory (TST) based rate law and the principle of detailed balancing from Aagaard and Helgeson (1982) and Lasaga (1984) with this assumption leads to very high precipitation rates even at low supersaturation (Hellevang and Aagaard, 2010). Comparisons of recent experiments on magnesite and dolomite dissolution and precipitation rates strongly suggests that growth rates at low supersaturation may be orders of magnitude lower than predicted through TST from corresponding dissolution rates (Hellevang and Aagaard, 2010). Whereas dissolution rates of dolomite and magnesite at 25 °C are fairly high (approximately 10^{-9} mole/m^2 s) (Pokrovsky et al., 2005), precipitation rates of disordered dolomite and magnesite at the same temperature are in practice zero (Arvidson and Mackenzie, 1997; Saldi et al., 2009). Moreover, the first order dependence on saturation state used for dissolution does not fit with the second order dependence of precipitation observed from the magnesite data of Saldi et al. (2009) or the higher order dependence seen for dolomite (Arvidson and Mackenzie, 1997). Similarly to magnesite, experiments of dawsonite show fast dissolution rates down to room temperatures (Hellevang et al., 2010), whereas dawsonite precipitation is slow even in highly supersaturated solutions at temperatures of 75–90 °C (Duan et al., 2005).

In this study, the rate equations suggested by Hellevang and Aagaard (2010) was used to revisit the potential for carbonate growth during CO_2 storage in Utsira type of reservoirs, i.e. low temperature quartz rich reservoirs. We simulated the carbonate potential case in which the CO_2 pressure was constant throughout the simulated 10,000 years. This would correspond to aqueous solutions residing approximate to the slow dissolving CO_2 plume trapped beneath some impermeable caprock structure (e.g., Gaus, 2010). The equations were used to explore how sensitive mineral carbonation was on rate parameters such as the reactive surface area for growth, the precipitation rate coefficient, and nucleation rates. Because dissolution rates are well known and trusted for many reservoir minerals, parameters for dissolution were not varied. Growth and nucleation rate data on the other hand are only partly known, and we therefore studied the sensitivity of growth and nucleation rate parameters on the carbonate growth. We then compared the results with the qualitative information available from natural analogues. Finally, we compared our results with previous published simulations on the long-term CO_2 mineral storage potential for the Utsira saline aquifer storage case at the Sleipner site. This work used the temperature, pressure and mineralogy reported for the Utsira Reservoir at the Sleipner injection site as a base case for the simulations.

2. Methods

2.1. Reaction rate equations

The most common way of modelling both mineral dissolution and precipitation rates is using a simplified form of the general transition-state-theory (TST) derived rate law as given by (Lasaga, 1981, 1984; Aagaard and Helgeson, 1977, 1982):

$$r_{+,-} = k_+ S \prod_i \mathbf{a}_i^{\nu_+} \exp\left(-\frac{Ea_+}{RT}\right) f(\Delta G_R) g(I), \quad (1)$$

where, r is reaction rate (mol/s), k_+ is the forward reaction rate coefficient (mol/m^2 s), S is the reactive surface area (m^2), $\mathbf{a}$ is the activity of species i affecting the rates, ν is the reaction order, Ea is the apparent activation energy, R is the gas constant and T is the absolute temperature. The functions f and g denote the dependence on the thermodynamic driving force and ionic strength, respectively. The $g(I)$ function is ignored in the following calculations. The thermodynamic driving force is usually simplified to:

$$f(\Delta G_R) = 1 - \exp\left(\frac{\Delta G_R}{RT}\right), \quad (2)$$

where ΔG_R is the free energy of the reaction and $\Omega = \exp(\Delta G_R/RT)$.

Because growth rates for minerals like magnesite (Saldi et al., 2009), calcite (Shiraki and Brantley, 1995), dolomite (Arvidson and Mackenzie, 1997, 1999) and quartz (Ganor et al., 2005) appear to be better represented by the non-linear part of the BCF (Burton Cabrera and Frank) crystal growth theory (Burton et al., 1951) than the TST, we divided the reaction rate equations into two affinity regions: (1) undersaturation following the TST approach (Eq. (1)) and (2) supersaturation following a simplified second-order BCF growth model. Moreover, because new carbonate phases requires heterogeneous nucleation preceding growth, we included a nucleation rate term based on classical nucleation theory (Nielsen, 1983; Walton, 1967):

$$J = k_N \exp\left\{-\beta N_A f(\theta)\left(\frac{v\sigma^{3/2}}{(RT)^{3/2} \ln \Omega}\right)^2\right\}, \quad (3)$$

where the pre-exponential factor k_N is the nucleation rate constant, β is a geometric shape factor, N_A is Avogadro's number, $f(\theta)$ is a correction factor for heterogeneous nucleation, v is molar volume, and σ is surface tension. This means that no nuclei will form at infinite low supersaturation and that fewer and larger nuclei forms at low temperatures and low supersaturation (Walton, 1967; Nielsen, 1983). We combined the BCF growth equation with a simplified form of the nucleation Eq. (3) to calculate the mineral formation rates:

$$r_- = -k_- S \prod_i \mathbf{a}_i^{\nu_-} \exp\left(-\frac{Ea_-}{RT}\right) \{\Omega - 1\}^2 - k_N \exp\left\{-\Gamma\left(\frac{1}{(T)^{3/2} \ln \Omega}\right)^2\right\}, \quad (4)$$

where Γ contains all parameters except T and Ω in the exponential term of Eq. (3). The reactive surface area for dissolution was calculated by:

$$S = \beta M n, \quad (5)$$

where β is the specific surface area, M is molar weight and n is the number of moles of the mineral. The reactive surface area for

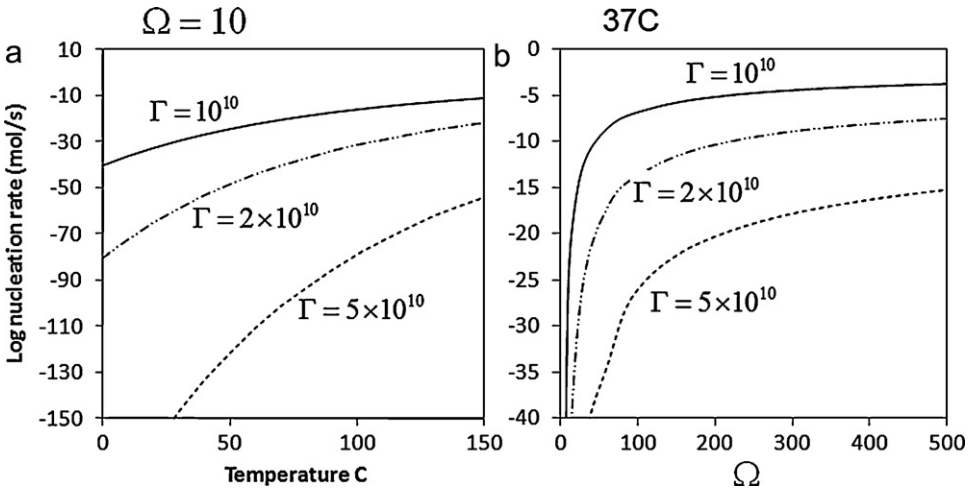

Fig. 1. Sensitivity on nucleation rates on the Γ parameter at (a) various temperatures and 10 times supersaturation (Ω = 10) and (b) various supersaturations at 37 °C. The simplified nucleation expression (last part of Eq. (4)) was used. Note that at 10 times supersaturation, significant nucleation rates require high temperatures, whereas nucleation rates increase rapidly upon increasing supersaturations.

precipitation was calculated by Eq. (5), but multiplied by λ defined as the dislocation surface density factor giving the fraction of the total surface area available for BCF growth.

As precipitation rate coefficients $k-$, growth reactive surface areas, and nucleation parameters of carbonates are to a large extent unknown, we ran a sensitivity study varying the parameters. The pre-exponential factor for nucleation, the nucleation rate coefficient $k_{N,}$ is a highly uncertain parameter, and values from 10^{10} to higher than 10^{30} nuclei per second have been used (Nielsen, 1983; Walton, 1967; Steefel and Van Cappelen, 1990). We chose an intermediate value of 10^{22} nuclei per second per kg water. To obtain k_N values as mole/s, we recalculated the nuclei/seconds values by assuming 1 nm spherical nucleii, a common density of 2.7 g/cm^3, and a common molar mass of 100 g/mol. Using these values, the k_N used for the base-case was estimated to 1 mole/s. This is a crude estimate, but as will be shown in the next sections, the nucleation rates and the potential for carbonate growth are little sensitive to changes in the values of the k_N. With a given choice of pre-exponential factor, proper values of Γ can be estimated from data obtained from nucleation rate experiments through the expression:

$$\Gamma = T^3 \ln(\Omega)^2\{\ln(\tau) + \ln(k_N)\}, \quad (6)$$

where τ is the retention time (s) before observed growth obtained from the nucleation rate experiments, and k_N is given as nucleus/second. Using this expression together with data of calcite nucleation from Verdoes et al. (1992), gives values of Γ between 10^9 and 10^{10}. As calcite nucleation and growth is orders of magnitude faster than other carbonates such as siderite, dolomite, and magnesite (e.g., Palandri and Kharaka, 2004), we used higher Γ values than estimated for calcite nucleation, with values ranging from 10^{10} to 5×10^{10}. This provided a large and reasonable range of nucleation rates for the given temperature and saturation states (Fig. 1). For the slowest reacting magnesian carbonates, magnesite and dolomite, we used $\Gamma = 4 \times 10^{10} \pm 10^{10}$, whereas for siderite and the other faster growing secondary phases we used $\Gamma = 2 \times 10^{10} \pm 10^{10}$. For ankerite, with a likely growth and nucleation rate between that of siderite and the magnesian carbonates, we used intermediate values of $\Gamma = 3 \times 10^{10} \pm 10^{10}$. Base-case precipitation rate coefficients for dawsonite and siderite were set equal to published dissolution rate coefficient, whereas the ankerite precipitation rate coefficient was unknown and chosen as intermediate between siderite and dolomite (Table 1). The sensitivity of mineral growth on the reactive surface area for growth, was examined by varying λ between 10^{-5}, reflecting a smooth surface with few dislocations, to one, meaning that the entire surface was reactive. Chalcedony was chosen to precipitate as a secondary phase because quartz is not expected to form at low temperatures. In typical diagenetic settings, quartz precipitation requires temperatures of 60–75 °C or higher to force aqueous silica activities down close to quartz saturation (e.g., Bjørlykke and Egeberg, 1993).

2.2. Thermodynamic data

The llnl.dat thermodynamic database included with the PHREEQC v2 numerical code (Parkhurst and Appelo, 1999), based on the thermo.com.V8.R6.230 database prepared at the Lawrence Livermore National Laboratory (Johnson et al., 1992), was used for the aqueous speciation and for most minerals. The fugacity coefficient of CO_2 was estimated according to the Soave–Redlich–Kwong (SRK) equation of state (Soave, 1972) and the solubility was adjusted for by a Poynting correction term. Both fugacity and poynting corrections were necessary to give good estimates of the solubility of CO_2 in PHREEQC as the ideal gas law was used in the numerical code. It has been shown earlier that the pre-calculated correction terms provide good estimates of the solubility of CO_2 for a range of salinities, temperatures and pressures (Hellevang and Kvamme, 2006).

Glauconite and ankerite thermodynamic data were not a part of the llnl.dat database, and were introduced in the model in this study separately. The thermodynamic properties of glauconite were based on Tardy and Duplay (1994). A low-temperature composition termed glauconite D with $\log K_{25\,^\circ C}$ value of 8.11 for the reaction was chosen as a representative member of the glauconite group minerals (Tardy and Duplay, 1994). Because the phase definitions in PHREEQC required charge balance and the composition of glauconite D in Tardy and Duplay (1994) was slightly off charge balance, we added 0.025 mole of Si to the original 3.71 in the structure and adjusted the $\log K_{25\,^\circ C}$ accordingly to 8.033. The adjustment of silica was chosen over other elements because the Si^{4+} charge ensured a minimum change in bulk chemistry compared to the reported values. The dissolution reaction was then defined as:

$$Ca_{0.02}K_{0.85}Fe_{1.03}Mg_{1.01}Fe_{0.05}Al_{0.32}Si_{3.735}O_{10}(OH)_2 + 7.06H+ = 0.02Ca^{2+} + 0.85K^+ + 1.03Fe^{3+} + 1.01Mg^{2+} + 0.05Fe^{2+} + 0.32Al^{3+} + 3.735SiO_2 + 4.53H_2O. \quad (7)$$

The next sections show that the glauconite stay far-from-equilibrium undersaturated for all simulations, with no simulated

Table 1
Mineral compositions and initial weight percent used for the model. These are the same minerals as reported by Chadwick et al. (2004), with additional minerals such as glauconite, magnetite, and pyrite as redox buffers.

Mineral	[a] $k_d^{37\,^\circ C}$ (mol/m^2 s)	[a] $k_p^{37\,^\circ C}$ (mol/m^2 s)	β BET (m^2/g)	References
Quartz	4.08×10^{-14}	4.08×10^{-14}		Tester et al. (1994)
Chalcedony	4.08×10^{-14}	4.08×10^{-14}	0.0225	Tester et al. (1994)
Albite	2.88×10^{-12}	2.88×10^{-12}	0.1	Brantley (2008)
K-feldspar	5.11×10^{-13}	5.11×10^{-13}	0.11	Brantley (2008) and Gautier et al. (1994)
Glauconite	4.788×10^{-10}	4.788×10^{-10}	0.0178	Tardy and Duplay (1994) and Aagaard et al. (2004)
Clinochlore-14A	2.8×10^{-12}	2.8×10^{-12}	1.6	Brandt et al. (2003) and Nagy (1995)
Smectite-high-Fe–Mg	5.59×10^{-14}	5.59×10^{-14}	50	Amram and Ganor (2005) and Golubev et al. (2006)
Kaolinite	1.85×10^{-13}	9.21×10^{-15}		Yang and Steefel (2008)
Muscovite	7.63×10^{-14}	7.63×10^{-14}	0.68	Oelkers et al. (2008)
Magnetite	2.398×10^{-9}	2.398×10^{-9}	0.102	White et al. (1994)
Pyrite	2.62×10^{-9}	2.62×10^{-9}	0.051	Williamson and Rimstidt (1994)
Calcite	Equilibrium	Equilibrium	–	
Ankerite	1.27×10^{-7}	1.00×10^{-12}	0.016	Arbitrary
Siderite	2.76×10^{-7}	2.76×10^{-7}	0.175	Golubev et al. (2009)
Magnesite	9.04×10^{-10}	1.94×10^{-16}	0.127	Pokrovsky et al. (2009) Saldi et al. (2009)
Disordered dolomite	1.27×10^{-7}	3.63×10^{-24}	0.016	Pokrovsky et al. (2005,2009) Arvidson and Mackenzie (1997)
Dawsonite	4.85×10^{-9}	4.85×10^{-9}	9.8	Hellevang et al. (2010)

[a] $k_d^{37\,^\circ C}$ and $k_p^{37\,^\circ C}$ are reaction rate coefficients for 37 °C estimated from cited rate data, apparent activation energies at pH 5.

values closer to equilibrium than 4 orders of magnitude undersaturation. The rate of dissolution was hence independent of the log K value, even if the stability would be increased by 10–15%. Natural ankerites are members of the dolomite-ankerite solid-solution series. They contain about 26–71 mol% of the $CaFe(CO_3)_2$ component, which appears to be the maximum possible iron content for any temperature. Standard state Gibbs free energy of formation and enthalpy of end-member $CaFe(CO_3)_2$ were 116.86 kJ/mol and −17.47 kJ/mol, respectively, from Woods and Garrels (1992). The ankerite composition chosen for the present work was $CaFe_{0.6}Mg_{0.4}(CO_3)_2$ which correspond to a solid solution of 0.4 dolomite and 0.6 ankerite.

2.3. The reservoir properties

The reservoir physical properties and mineralogy were chosen as typical for cold quartz-dominated non-consolidated sand and was based on reported data for the Utsira reservoir at the Sleipner CO_2 injection. At a present-day depth of 700–1000 m, the temperature of the Utsira Sand is approximately 37 °C, and the pressure in the reservoir is 100 bar. A volume of rock containing 1 kg of formation water was modelled. Taking into account a porosity of 35% (Chadwick et al., 2004) and an estimated solid density of 2.65 kg/l, therefore, the rock unit can be said to contain 1 kg of pore water and 4.91 kg solid rock or 1.86 l of solid phase. The system was assumed fully water saturated and in contact with an infinite CO_2 reservoir.

Macroscopic and microscopic analysis of core and cutting samples of the Utsira Sand has revealed a composition consisting primarily quartz with some feldspar and shell fragments. Sheet silicates are present in small amounts. Chadwick et al. (2004) did not determine the clay mineral composition, but reported a few per cents (ca. 3%) of total clay in the Utsira Sand. In our base case model, the total of clay minerals was assumed to be 4%. Because glauconite is a common mineral in the central and northern part of the Utsira Sand (Gregersen and Johannessen, 2007), and glauconite may be an important source of iron and magnesium for forming carbonate minerals, we included 1% glauconite as representative for Fe–Mg mica.

The choice of redox conditions and the resulting distribution of redox sensitive elements was based on the general geochemical control on burial diagenesis discussed previously by Aagaard and Egeberg (1998). The pyrite-magnetite buffer has been predicted for such reservoirs based on concentrations of H_2S (Aagaard et al.,

Table 2
Formation water composition in Utsira sand selected from Oseberg field and adjusted to be compatible with the Utsira reservoir conditions (Johnson et al., 2004).

Mineral	Chemical formula	wt.%
Primary		
Quartz	SiO_2	72.5
Chalcedony	SiO_2	0
Albite	$NaAlSi_3O_8$	3.0
K-feldspar	$KAlSi_3O_8$	13.0
Glauconite D	$Ca_{0.02}K_{0.85}Fe_{1.03}Mg_{1.01}Fe_{0.05}Al_{0.32}Si_{3.735}O_{10}(OH)_2$	1.0
Clinochlore-14A	$Mg_5Al_2Si_3O_{10}(OH)_8$	0.4
Smectite-high-Fe–Mg	$Ca_{0.025}Na_{0.1}K_{0.2}Fe_{0.5}Fe_{0.2}Mg_{1.15}Al_{1.25}Si_{3.5}H_2O_{12}$	0.6
Kaolinite	$Al_2Si_2O_5(OH)_4$	1.0
Muscovite	$KAl_3Si_3O_{10}(OH)_2$	2.0
Magnetite	Fe_3O_4	0.1
Pyrite	FeS_2	0.4
Calcite	$CaCO_3$	6.0
Secondary		
Ankerite	$CaFe_{0.6}Mg_{0.4}(CO_3)_2$	0
Siderite	$FeCO_3$	0
Disordered dolomite	$CaMg(CO_3)_2$	0
Magnesite	$MgCO_3$	0
Dawsonite	$NaAlCO_3(OH)_2$	0

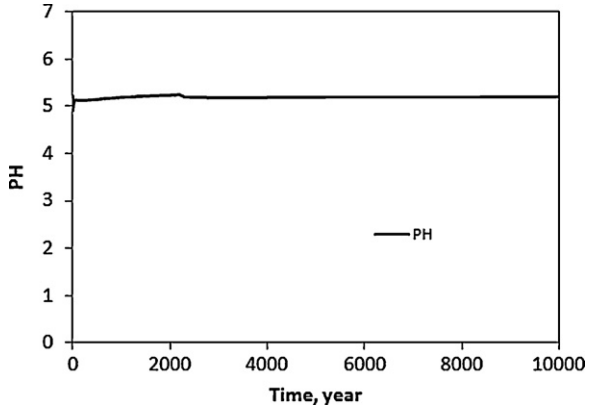

Fig. 2. The CO_2 charged water in equilibrium with calcite adjusts to an initial pH of 4.8. The pH of the system during 10 000 years simulation is roughly 5 (base case).

2001). Magnetite and pyrite were introduced in small fractions in this model to play a role as redox buffers. A pyrite fraction of 1% has been reported in the shale layers in the vicinity of Sleipner (Chadwick et al., 2004). In our model we used pyrite and magnetite volume fractions of 0.4% and 0.1%, respectively. The mineral compositions and initial weight percentage used in the model are listed in Table 2.

The selection of possible secondary carbonate minerals used in the model was conducted after investigating the saturation indices of all carbonate minerals in the PHREEQC v2 llnl.dat database and ankerite. The simulation showed that the only carbonates necessary to consider as secondary phases were ankerite, disordered dolomite, dawsonite, siderite and magnesite, because they were close to saturation or supersaturated. All other hydrous magnesium carbonate minerals such as hydromagnesite ($Mg_5(CO_3)_4(OH)_2{:}4H_2O$), lansfordite ($MgCO_3{\cdot}5H_2O$) and nesquehonite ($MgCO_3{\cdot}3H_2O$) were strongly undersaturated during the timeframe of 10 000 years. The secondary minerals are included in Table 2.

The formation water composition listed in Table 3 was chosen on the basis of values reported from Utsira at Oseberg, about 200 km north of Sleipner (Gregersen et al., 1998). The value was adjusted

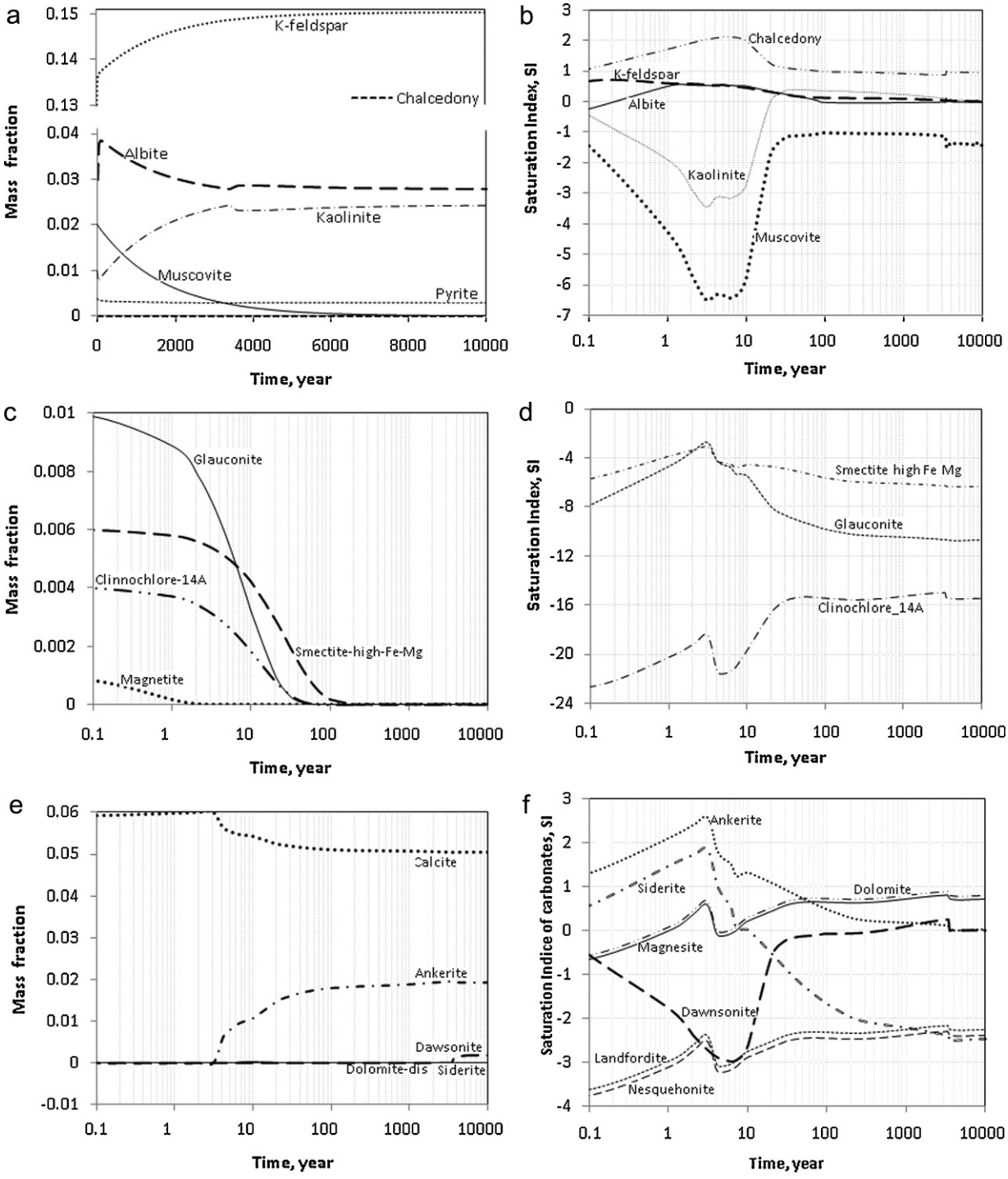

Fig. 3. Mineral reactions following the CO_2 perturbation for the base-case simulation ($\Gamma = 2.0 \times 10^{10} - 4.0 \times 10^{10}$, $k_N = 1$). Left (a, c, and e) are the temporal evolution of mineral mass fractions of slow reacting silicates (a), fast reacting silicates and magnetite (c) and carbonates (e). Right column shows the corresponding saturation states $SI = \log(\Omega)$.

Table 3
Kinetic parameters used for rate calculations.

Component	mole/kg water
Na	4.52×10^{-1}
K	5.30×10^{-3}
Ca	7.42×10^{-3}
Mg	1.81×10^{-2}
Al	1.30×10^{-8}
Cl	5.21×10^{-1}
HCO_3	2.32×10^{-3}
$SiO_{2,aq}$	1.66×10^{-4}
pH	6.5

for representing in situ Utsira reservoir condition according to the constraints given by Johnson et al. (2004).

2.4. Numerical method

Calculation of mineral reaction rates, CO_2 phase equilibrium, and aqueous speciation were carried out using the numerical model code PHREEQC-2 (Parkhurst and Appelo, 1999). Parameters for the reaction rate equations were defined individually for all mineral reactions in the input file and solved by the PHREEQC code Ordinary Differential Equation (ODE) solver which is based on Backward Differentiation formula (BDF) methods suitable for the Stiff systems of equations.

3. Results

After CO_2 was injected into the reservoir, it dissolved in the water and reduced the pH to approximately 3.3. The pH was, however, immediately adjusted to 4.9 as the CO_2 charged solution was forced into equilibrium with calcite. After that, the subsequent mineral reactions increased the pH only slightly and the pH stayed at around five for the entire simulation time (Fig. 2).

3.1. Base case simulation: silicate dissolution and carbonate precipitation

Following the perturbation of the system by the CO_2 injection, the pH dropped and most of the silicates present in the reservoir became unstable. Albite and muscovite dissolved slowly and provided potassium, silica and aluminium for kaolinite and K-feldspar growth (Fig. 3a). Albite gradually ceased to dissolve as the mineral approached saturation (Fig. 3b), whereas all muscovite was dissolved after approximately 8000 years. After a few years chalcedony formed steadily but at a small amount at slightly more than 10 times supersaturation (Fig. 3b). The less abundant but more important minerals for solid carbonate storage, glauconite, smectite and chlorite, dissolved fast and was completely dissolved after approximately 100–200 years (Fig. 3c). The saturation indices show that these minerals stayed grossly undersaturated (Fig. 3d) and that the dissolution hence was steady and independent of the thermodynamic driving force term of Eq. (1). The dissolution of the clay minerals released large amounts of Mg^{2+} and Fe^{2+} within decades, and therefore ankerite precipitated (Fig. 3e). Calcium ions for the ankerite growth were supplied from calcite dissolution (Fig. 3e). Once glauconite and smectite completely dissolved, ankerite no longer formed in large amounts due to the cessation in supply of iron and magnesium (Fig. 3e). Dawsonite formed after approximately 2000 years after reaching a slight supersaturation (Fig. 3e and f), but the amount was limited by the modest amount of albite dissolved at the high silica activity.

The results at the end of 10 000 years showed that the net CO_2 trapped in solid phase, mostly ankerite, after subtracting the dissolved calcite made up a total of ca. 1.2% of the total mineral content.

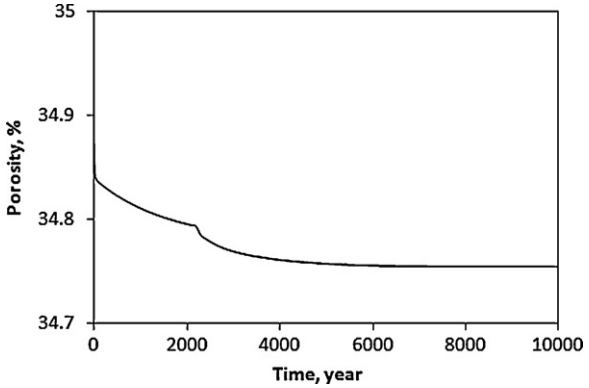

Fig. 4. Porosity changes following the CO_2 injection. The porosity reduction after 10 000 years is small because the density of the dissolving and precipitating phases are similar.

The effect of the CO_2 sequestration on the porosity, however, was much smaller. Because the density differences between the minerals included were small, the replacement of clay minerals, albite and calcite with the secondary minerals reduced the porosity by only 0.23%, from 35% to 34.77% (Fig. 4).

3.2. The Sensitivity of carbonate formation on Γ

The gamma parameter, Γ in Eq. (4), contains the dependence of nucleation rate on reservoir-specific properties like surface tensions and geometric properties of the nuclei (see Eqs. (3) and (4)). At present, little information is available about the nucleation rates of carbonates like magnesite, ankerite, dawsonite and dolomite in sedimentary basin systems. As is evident from Fig. 1b, nucleation rates at low supersaturations are highly sensitive to Γ, whereas the nucleation rates show less dependence on Γ as the supersaturation increases. We chose to vary the base-case values by $\pm 10^{10}$, giving a large range of nucleation rates at 37 °C.

At the lowest value of gamma, giving high nucleation rates at low supersaturation, siderite formed after approximately 1 year but was later (at 20 years) replaced by ankerite (Fig. 5a). The amount of dawsonite was similar to the base-case (Fig. 5b) and the total carbon stored given by ankerite and dawsonite was therefore similar (Fig. 5a and b). Using the highest value of gamma gave close to the same results as for the base-case. The supersaturation needed to precipitate ankerite was shifted to a slightly higher value (Fig. 5d and f), and the growth of ankerite was therefore delayed by approximately 1 year. The total amount of carbonate stored was very similar to the base-case. The weak sensitivity on carbonate growth on the gamma nucleation rate parameter can be explain by the similarity in nucleation rates at a range of gamma at high supersaturations (Fig. 1b).

3.3. Sensitivity of carbonate formation on the precipitation rate coefficients k_-

Slow growth rates of minerals like magnesite and dolomite at low temperatures may suggest that other magnesian carbonates, like ankerite, may also be prevented from forming at low temperatures. Moreover, the rare occurrences of dawsonite as a replacement product in natural CO_2 storage analogues may suggest that this mineral is kinetically prevented from growth as well. Therefore, because the BCF growth rates are unknown for ankerite and dawsonite, we chose to explore how sensitive the potential of carbonate growth was on the precipitation rate coefficients of these two minerals. We reduced the k_- from the base-case values by three and five orders of magnitude. All other rate parameters were kept constant.

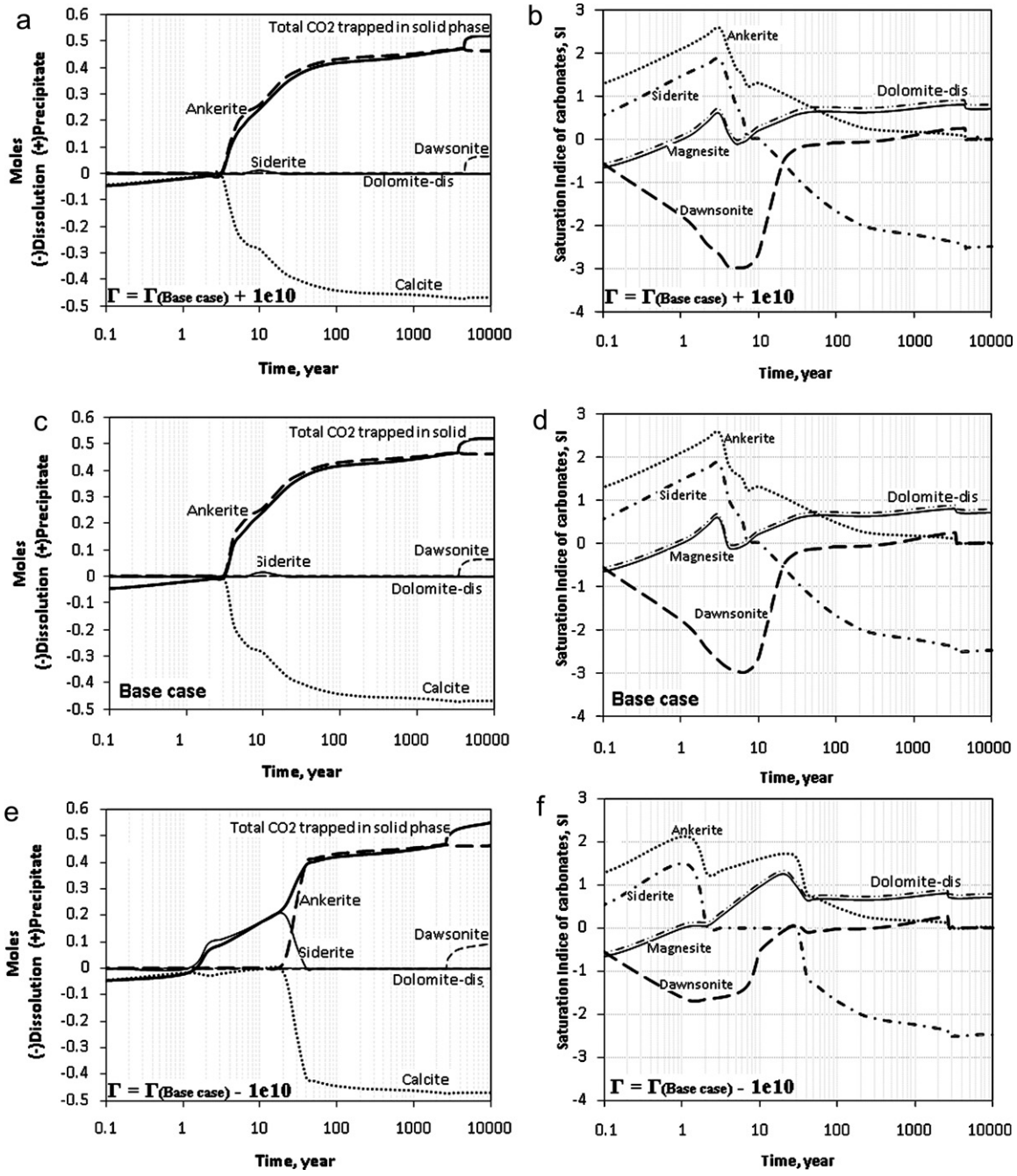

Fig. 5. Sensitivity of the nucleation rate parameter Γ (Eq. (4)) on the CO_2–mineral–water interactions. Values were varied $\pm 10^{10}$ from the base case.

A reduction of the dawsonite and ankerite growth rate coefficients by three orders of magnitude reduced the total amount of carbonate that formed by approximately 10% compared to the base-case. The secondary carbonate assemblage was changed from ankerite and dawsonite to siderite and dawsonite (Fig. 6c and d). However, after 5000 years, ankerite started to grow replacing the earlier formed siderite. Moreover, although the dawsonite rate was lowered by three orders of magnitude, more dawsonite formed as it stayed longer at higher supersaturation. A further two orders of magnitude reduction in the precipitation rates, gave a similar result, but dawesonite growth was postponed as it required higher supersaturation, and no ankerite formed to replace the siderite (Fig. 6e and f). The total amount of carbonate formed at the end of the simulated time was in this case further lowered as no magnesium or calcium was trapped in ankerite (Fig. 6e).

3.4. Sensitivity of carbonate formation on the dislocation surface density factor λ

The reactive surface area for growth is one of the largest uncertainties in predicting the potential for mineral formation. Implicit given in our use of a BCF-type growth rate expression with a second-order dependence on reaction affinity, is that the macroscopic rates are given by growth at screw dislocations. We thus defined a dislocation surface density factor λ with values between 1 and 10^{-5} and multiplied this with the total growth surface area. A value of 1 implies that the entire surface area, calculated from the mass and specific surface area (Eq. (5)), was available for growth, whereas a value of 10^{-5} implies a smooth surface with few dislocations and hence a strongly reduced growth rate. The effect of varying λ has the same effect as changing the reaction rate coefficient as the rate

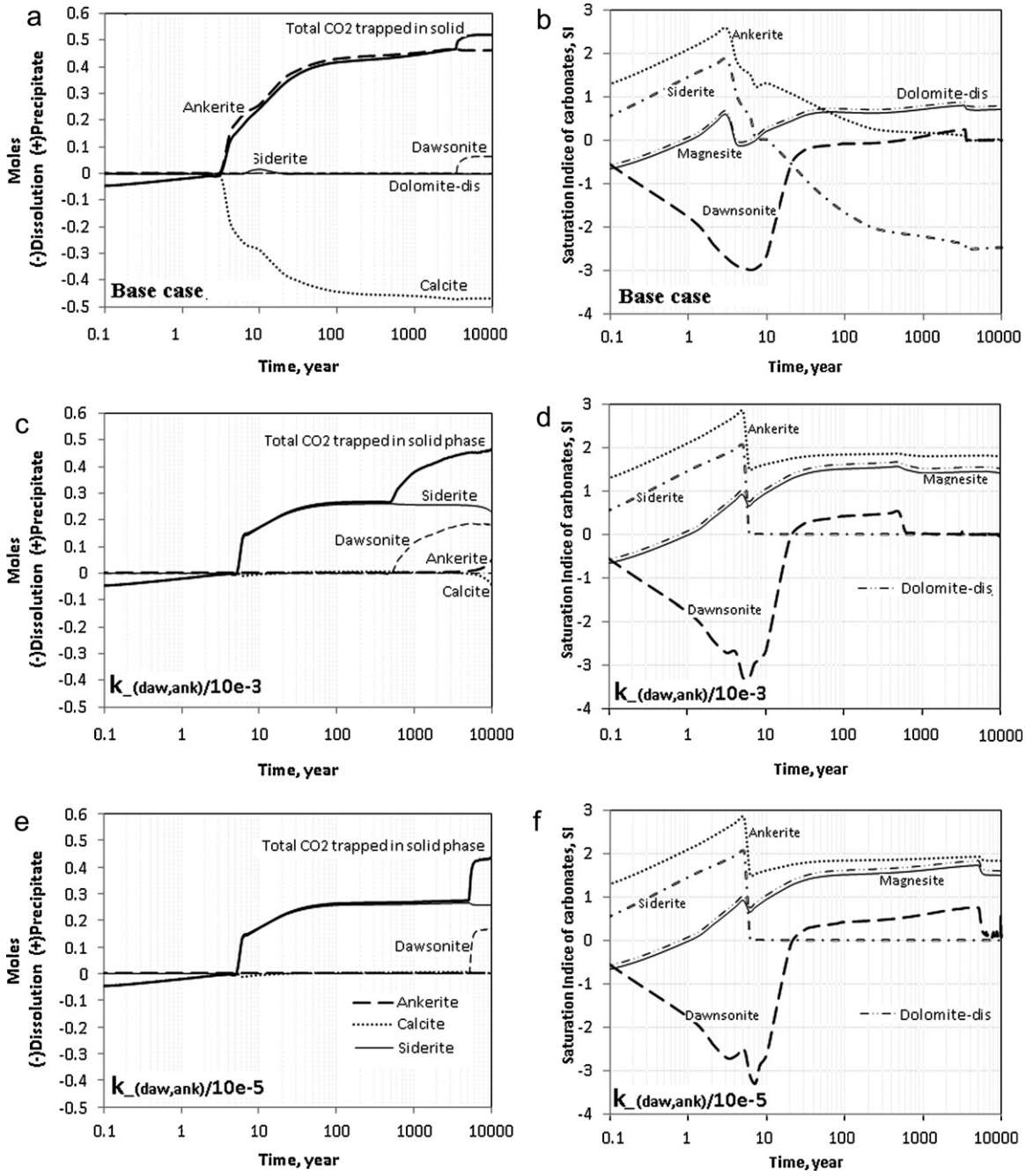

Fig. 6. The sensitivity of mineral carbonation on the precipitation rate coefficient k_{-} for minerals with unknown growth rates. The k_{-} was reduced by three (a) and five (b) orders of magnitude relative to the base-case (Table 1). The precipitation rate coefficients for magnesite and dolomite were known from Saldi et al. (2009) and Arvidson and Mackenzie (1997) respectively and were not varied.

is given by the product of these two. However, because the growth rate coefficient was not only varied for ankerite and dawsonite (previous section), the sensitivity of λ served to give some additional information on the timing and nature of carbonate growth.

At a one orders of magnitude reduction of λ (λ = 0.1), the initiation of ankerite growth was postponed from two to five years reflecting the higher supersaturation needed at lower precipitation rates (Fig. 7a–d). Siderite formed as an intermediate phase between 10 and 100 years before it dissolved and was replaced by ankerite (Fig. 7b). Further reduction of λ to three orders of magnitude relative to the base-case resulted in a early siderite growth and ankerite did not form (Fig. 7c). More dawsonite formed in this case relative to the base-case (Fig. 7a and c). Finally, at five orders of magnitude lower λ relative to the base-case, siderite growth was delayed to three years (Fig. 7d). The total amount of CO_2 stored at the final stage was approximately 20% lower for the last case compared to the base-case (Fig. 7a and d).

3.5. Sensitivity of carbonate formation on the nucleation rate coefficient k_N

Because the nucleation rate coefficient k_N is highly uncertain and not exactly known for the secondary minerals, we varied it by ±3 orders of magnitude from the base-case 1 mole/s at the highest value of gamma ($+10^{10}$ from base-case). Fig. 8 shows however that changes in the k_N value by ±3 orders of magnitude has no significant

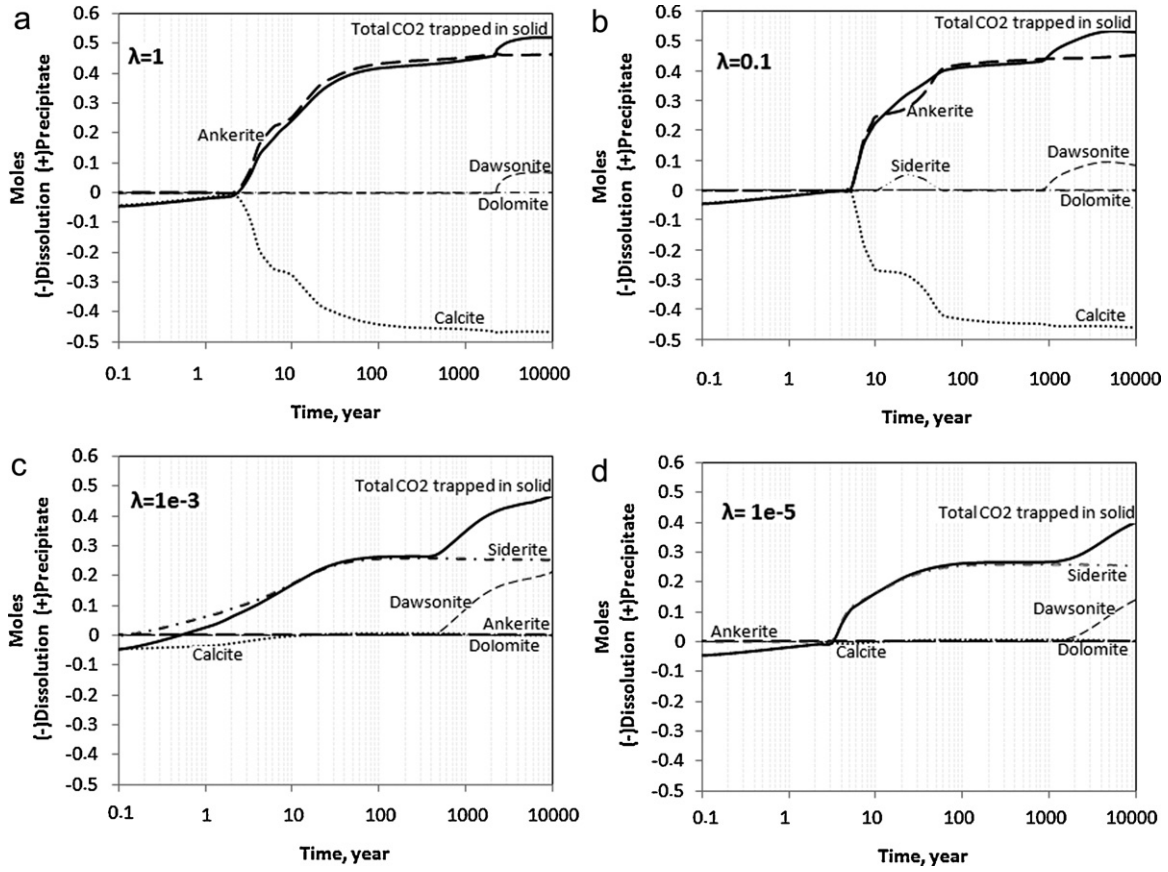

Fig. 7. Sensitivity of the surface dislocation density factor λ on the mineral carbonation. Values of λ were varied between one, meaning that the full surface was used as reactive surface, down to 10^{-5}, meaning a smooth surface with few dislocations and hence mostly nucleation-driven reactions.

effect on the timing and amount of secondary carbonates that form, and further analyses of the sensitivity of carbonate growth on k_N was hence not done.

4. Discussion

4.1. Are predictions of growth rates from far-from-equilibrium dissolution rates valid?

The "conventional" method of simulating CO_2 mineral storage constrained by mineral reaction rates has been to use a common TST-derived rate equation for both dissolution and precipitation with parameters obtained from far-from-equilibrium dissolution rate experiments (e.g., Gaus et al., 2005; Johnson et al., 2004; Knauss et al., 2005; Xu et al., 2004, 2007). Experiments on the dissolution and precipitation rates of carbonates (e.g., Saldi et al., 2009; Arvidson and Mackenzie, 1997) as well as theoretical considerations of mechanisms responsible for the rates (e.g., Nagy and Lasaga, 1992; Lüttge et al., 2003; Fischer and Lüttge, 2007; Dove and de Yoreo, 2010; Lüttge and Arvidson, 2010; Arvidson and Lüttge, 2010), may however suggest that the use of far-from-equilibrium derived TST dissolution rate parameters for precipitation is not justified.

One recent example is the reaction rates of magnesite. Far-from-equilibrium dissolution rate experiments by Pokrovsky et al. (2009) suggested a 100 °C pH 8 reaction rate of approximately 10^{-8} mole/m^2 s. Using the TST-derived Eq. (1) with this reaction rate coefficient, unit reactive surface and two times supersaturation ($\Omega = 2$) results in an estimated precipitation rate of 10^{-8} mole/s. Recent experiments on magnesite precipitation rates (Saldi et al., 2009) however showed that at 100 °C, pH approximately 8–8.5, supersaturation equivalent to larger than 10 kJ/mol (corresponding to more than 25 times supersaturation) was required to achieve the same precipitation rates. Moreover, apparent activation energies that may reflect the mechanisms responsible for the rates were strikingly different. Pokrovsky et al. (2009) reported an apparent activation energy for magnesite dissolution of 34 kJ/mol whereas Saldi et al. (2009) reported 159 kJ/mol for magnesite precipitation. The consequence is that, as shown in the present simulations, the difference between dissolution and precipitation may be even much larger at low temperatures such as for the Utsira reservoir (37 °C). For dawsonite, previously suggested to be a significant permanent or intermediate storage host (Johnson et al., 2004; Knauss et al., 2005; Xu et al., 2004, 2007; Zerai et al., 2006), similar differences between dissolution and precipitation rates are likely. Dawsonite shows fast dissolution rates down to room temperatures (Hellevang et al., 2010), whereas precipitation rate experiments by Duan et al. (2005) show slow rates at strongly supersaturated solutions (2000 times) at 75–90 °C (Hellevang and Aagaard, 2010). Finally, the affinity dependence of growth rates for minerals like magnesite (Saldi et al., 2009), calcite (Shiraki and Brantley, 1995), dolomite (Arvidson and Mackenzie, 1997, 1999) and quartz (Ganor et al., 2005) appear to be better explained by growth models such as the BCF (Burton Cabrera and Frank) crystal growth theory (Burton et al., 1951) than the TST.

4.2. Information on mineral storage from natural CO_2 analogues

Formation of carbonates such as ankerite and dolomite in CO_2 charged reservoirs is supported by the observation of natural analogues such as the Sleipner Vest gas condensate field (Ranaweera, 1987), the Upper Jurassic reservoir sandstones of the Magnus in

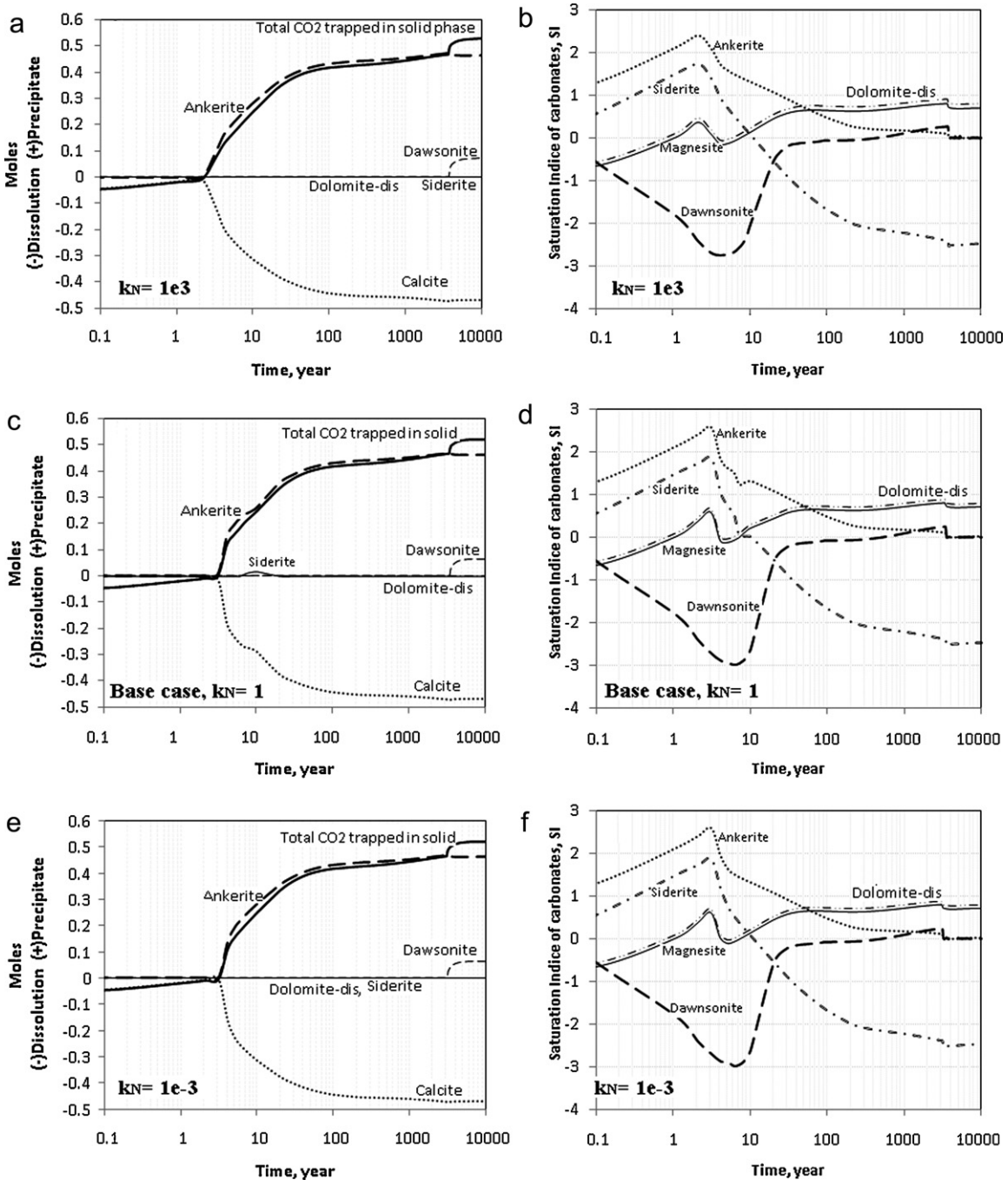

Fig. 8. Sensitivity of the nucleation rate coefficient k_N on the amount of carbonates formed (a, c, and e) and on the corresponding saturation indices (b, d, and f). Values were varied ±3 orders of magnitude from the base-case 1 mole/s.

North Sea (Baines and Worden, 2004; Macaulay et al., 1993), the Miller in North Sea (Lu et al., 2009), the Ladbroke in Australia (Watson et al., 2004), and Montmiral in France (Pauwels et al., 2007). The formation of dolomite is however limited to higher temperatures than for the cold 37 °C Utsira-type reservoir, and even at more than 1000-fold oversaturation over 32 years, laboratory experiments at room temperature has failed to form dolomite (Land, 1998). Arvidson and Mackenzie (1997, 1999) showed that high apparent activation energies for dolomite growth explains the general lack of dolomite formation at low temperatures. The same high apparent activation energies was shown for magnesite by Saldi et al. (2009). In general, precipitation of magnesian carbonates requires dehydration steps breaking of the strong hydration shell surrounding magnesium ions (Arvidson and Mackenzie, 1999; Deelman, 2001), and minerals like dolomite and magnesite is for that reason not expected to form in low-temperature reservoirs. It is therefore also questionable if ankerite will form at the 37 °C conditions at the Utsira reservoir, and the potential for carbonate growth may be given by carbonates such as siderite or hydrous magnesium carbonates.

Dawsonite is reported to be abundant in natural reservoirs that are currently at a high CO_2 pressure, or that have previously experienced an influx of CO_2 (Smith and Milton, 1966; Baker et al., 1995; Moore et al., 2005; Worden, 2006; Golab et al., 2006, 2007; Gao et al., 2009). By its elevated thermodynamic stability at highly alkaline conditions (e.g., Hellevang et al., 2005), dawsonite is com-

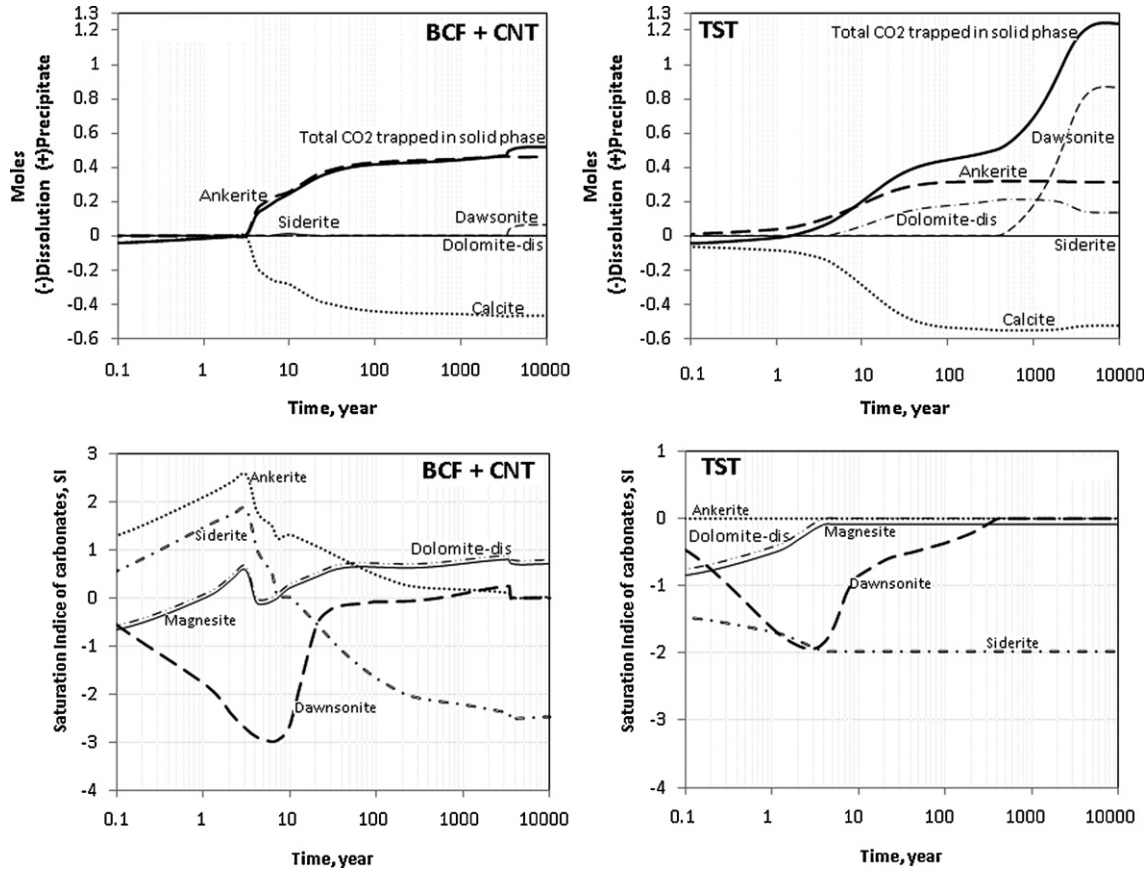

Fig. 9. Comparison of carbonate mineral changes (a and b) and corresponding saturation states (c and d) between the current BCF + CNT model and the traditionally used TST-derived model. The largest difference between the models is the formation of dolomite and dawsonite, which forms a high fraction of the secondary carbonates using the TST-model.

monly found associated with $NaHCO_3$-elevated brines reacting with alumino-containing minerals. One example of extensive dawsonite formation from such highly alkaline solutions is the Green River Formation of Colorado (Smith and Milton, 1966). Dawsonite is found together with analcime ($NaAlSi_2O_6{\cdot}H_2O$) and carbonates such as nahcolite ($NaHCO_3$), both indicating highly alkaline conditions. Dawsonite may also form at acidic conditions such as in the Triassic Lam Formation in the Shabwa Basin, Yemen, where it is found at concentrations of up to 8% of the sediment (Worden, 2006). Detailed petrological investigations suggest that at temperatures from 85 °C to 100 °C, feldspars have reacted with CO_2 and high-NaCl brines formed dawsonite together with quartz. Albite in perthitic feldspars have been replaced by dawsonite whereas the potassium part remained unaltered (Worden, 2006). Similar reactions have been observed for the Hailaer Basin in Northeastern China where feldspars in arkoses and lithic arkoses have been replaced by dawsonite and micro quartz by interaction with CO_2 and waters at temperatures between 85 °C and 105 °C (Gao et al., 2009). Dawsonite was in this case interpreted as a late-stage diagenetic mineral following illite and kaolinite formation. Although dawsonite is abundant locally as in the Green River and Lam Formations, it is not always present after long-term interactions between sediments and aqueous solutions at high CO_2 pressures. For example, Gaus et al. (2004) examined mineral reactions following long-term interactions with CO_2 for the Montmiral, Southeast Basin, France, at present-day 100 °C and 360 bar, and Messokampos, Florina Basin, Greece, at maximum 10 bar and 43 °C (Gaus et al., 2004). The Montmiral reservoir contains high-NaCl brines with salinities of about 3 times seawater, and K-feldspar that could act as an aluminium source for dawsonite growth. Analyses of the Montmiral waters suggest that dawsonite is close to saturation or slightly supersaturated (Pauwels et al., 2007). No dawsonite has however been observed (Gaus et al., 2004; Pauwels et al., 2007). The Messokampos reservoir has lower salinity than seawater, but abundant Na-feldspar and the high pH of 8.7 should in this case favor dawsonite growth. The fairly low NaCl content of the waters and the low temperatures and CO_2 partial pressures are probably the reason for the lack of dawsonite growth in this case. Another example of natural CO_2-charged reservoir that appears to lack dawsonite growth is found in the shallow Bravo Dome natural CO_2 field in New Mexico (Pearce et al., 1996). Detailed petrographic studies shows extensive corrosion of plagioclase from CO_2-charged acidified waters and formation of authigenic minerals. No dawsonite was observed.

4.3. *What do the TST-derived equations predict for the Utsira-type system?*

Previous numerical simulations of the potential of carbonate mineral storage in the Utsira Sand are limited to the 20 and 10,000 years 2D reactive transport models reported by Audigane et al. (2007) and Johnson et al. (2004) respectively, and the 18.000 years 3D reactive flow simulations reported in Thibeau et al. (2007). These three simulations and the present work agree well on the limited effect of the mineral reactions on porosity, and all produced similar pH evolution ending up at pH 5, mainly buffered by the carbonate reactions. One of the large differences between the current and earlier work is that, for the earlier simulations, minerals were allowed to precipitate as soon as an infinitesimal supersaturation were reached, and TST-derived equations with rate data derived from dissolution rate experiments were used (see review

by Gaus, 2010). This allowed rapid growth at small oversaturations and the formation of unrealistic large amounts of minerals such as dawsonite, magnesite, and dolomite.

To allow a direct comparison between the current BCF + CNT rate model and TST, we simulated the same base-case system, but used the TST-derived Eqs. (1), (2) and (5) using the dissolution rate data in Table 1. The resulting temporal changes in moles of carbonates for the two rate models are shown in Fig. 9a and b, and the corresponding saturation states are shown in Fig. 9c and d. The largest difference between the two models, which agree with earlier simulations of the Utsira system, is the formation of dolomite and eventually dawsonite as the dominant secondary phase when using a TST model (Fig. 9a and b). In addition, because of the increased amount of dawsonite formed, the total amount of carbonate formed is more than doubled (Fig. 9a and b). A comparison of the saturation states shows that the BCF + CNT model allows some degree of supersaturation before growth, whereas the TST model predicts rapid precipitation very close to saturation.

4.4. Limitations of the BCF + CNT model

At present we lack experimental data on the precipitation rates of carbonate minerals such as ankerite and we lack detailed knowledge on nucleation rates for most minerals. Such data, in addition to more data on clay mineral dissolution rates and on the abundance and distribution of the reacting phases, are clearly necessary in order to better understand the potential for mineral carbonate storage of CO_2. Moreover, even though the present BCF + CNT model represents an improvement from the earlier used TST-derived models, AFM studies of mineral growth, such as by Teng et al. (2000), indicate that no simple model exists that can provide a general predictive tool that governs all physical and chemical conditions that is encountered for mineral growth following CO_2 storage.

5. Conclusions

The use of TST-derived equations to predict carbonate growth, using one set of kinetic parameters derived from far-from-equilibrium dissolution rate experiments, is suggested to largely overestimate the growth potential for carbonates such as dolomite, magnesite, and dawsonite. On the other hand, if a mixed-carbonate such as ankerite forms, the long-term potential will be given by the amount of smectite and glauconite or other reactive clay minerals available in the reservoir, independent of which model was used. We found that the timing of significant carbonate growth was highly sensitive to nucleation rates. At high nucleation rates, lower supersaturation was required before carbonate phases grew, whereas growth required higher supersaturation at low nucleation rates. The exact composition of the secondary-mineral assemblage, which is essential in order to understand natural analogues, is dependent on growth and nucleation rate parameters that at present are largely unknown. There is thus a large need for experimental data on nucleation and growth for possible secondary minerals like ankerite, siderite and dawsonite.

Acknowledgements

We appreciate valuable and interesting discussions during the Goldschmidth 2010 conference in Knoxville, TN, and we would like to thank Amy Dale for helping us to correct the language in an earlier version of the manuscript. The study was made possible through financial supported by the Research Council of Norway through project SSC-Ramore (NFR 178008/I30).

References

Aagaard, P., Egeberg, P.K., 1998. Formation water and diagenetic modifications: General trends exhibited by oil fields from the Norwegian shelf. A model for formation waters in oil prone subsiding basins. In: Arehart, G.B., Huston, J.R. (Eds.), Water–Rock Interaction, WRI-9. Balkema, pp. 281–286.

Aagaard, P., Helgeson, H.C., 1977. Thermodynamic and kinetic constraints on the dissolution of feldspars. Geological Society of America, Abstract with programs v. 9, p. 873.

Aagaard, P., Helgeson, H.C., 1982. Thermodynamic and kinetic constraints on reaction rates among minerals and aqueous solutions I. Theoretical considerations. American Journal of Science 282, 237–285.

Aagaard, P., Jahren, J.S., Ehrenberg, S.N., 2001. H2S-controlling reactions in clastic hydrocarbon reservoirs from the Norwegian Shelf and Gulf Coast. In: Cindu, R. (Ed.), Water–Rock Interaction, WRI-10. Balkema, pp. 129–132.

Aagaard, P., Oelkers, E.H., Schott, J., 2004. Glauconite dissolution kinetics and application to CO_2 storage in the subsurface. Geochimica Et Cosmochimica Acta 68 (11), A143–A1143.

Amram, K., Ganor, J., 2005. The combined effect of pH and temperature on smectite dissolution rate under acidic conditions. Geochimica et Cosmochimica Acta 69 (10), 2535–2546.

André, L., Audigane, P., Azaroual, M., Menjoz, A., 2007. Numerical modeling of fluid–rock chemical interactions at the supercritical CO_2–liquid interface during CO_2 injection into a carbonate reservoir, the Dogger aquifer (Paris Basin, France). Energy Conversion and Management 48 (6), 1782–1797.

Arvidson, R.S., Mackenzie, F.T., 1997. Tentative kinetic model for Dolomite precipitation rate and its application to Dolomite distribution. Aquatic Geochemistry 2, 273–298.

Arvidson, R.S., Mackenzie, F.T., 1999. The dolomite problem: control of precipitation kinetics by temperature and saturation state. American Journal of Science 299, 257–288.

Arvidson, R., Lüttge, A., 2010. Unification of growth and dissolution models: a carbonate example. Geochimica et Cosmochimica Acta 74 (11 (Suppl. 1)), A34.

Assayag, N., Matter, J., Ader, M., Goldberg, D., Agrinier, P., 2009. Water–rock interactions during a CO_2 injection field-test: implications on host rock dissolution and alteration effects. Chemical Geology 265 (1–2), 227–235.

Audigane, P., Gaus, I., Czernichowski-Lauriol, I., Pruess, K., Xu, T., 2007. Two-dimensional reactive transport modeling of CO_2 injection in a saline aquifer at the Sleipner site, North Sea. American Journal of Science 307 (7), 974–1008.

Bachu, S., Bonijoly, D., Bradshaw, J., Burruss, R., Holloway, S., Christensen, N.P., Mathiassen, O.M., 2007. CO_2 storage capacity estimation: methodology and gaps. International Journal of Greenhouse Gas Control 1 (4), 430–443.

Baines, S.J., Worden, R.H., 2004. The long-term fate of CO_2 in the subsurface: natural analogues for CO_2 storage. Geological Society, London, Special Publications 233 (1), 59–85.

Baker, J.C., Bai, G.P., Hamilton, P.J., Golding, S.D., Keene, J.B., 1995. Continental-scale magmatic carbon dioxide seepage recorded by dawsonite in the Bowen-Gunnedah-Sydney Basin system, Eastern Australia. Journal of Sedimentary Research A65 (3), 522–530.

Bjørlykke, K., Egeberg, P.K., 1993. Quartz cementation in sedimentary basins. The American Association of Petroleum Geologists Bulletin 77 (9), 1538–1548.

Brandt, F., Bosbach, D., Krawczyk-Bärsch, E., Arnold, T., Bernhard, G., 2003. Chlorite dissolution in the acid ph-range: a combined microscopic and macroscopic approach. Geochimica et Cosmochimica Acta 67 (8), 1451–1461.

Brantley, S.L., 2008. Kinetics of mineral dissolution. In: Brantley, S.L., Kubicki, J.D., White, A.F. (Eds.), Kinetics of Water–Rock Interaction. Springer Science business Media, LLC, New York, pp. 151–196.

Burton, W.K., Cabrera, N., Frank, F.K., 1951. The growth of crystals and the equilibrium structure of their surfaces. Philosophical Transactions of the Royal Society of London 243, 299–358.

Cantucci, B., Montegrossi, G., Vaselli, O., Tassi, F., Quattrocchi, F., Perkins, E.H., 2009. Geochemical modeling of CO_2 storage in deep reservoirs: the Weyburn Project (Canada) case study. Chemical Geology 265 (1–2), 181–197.

Chadwick, R.A., Zweigel, P., Gregersen, U., Kirby, G.A., Holloway, S., Johannessen, P.N., 2004. Geological reservoir characterization of a CO_2 storage site: the Utsira Sand, Sleipner, northern North Sea. Energy 29 (9–10), 1371–1381.

Deelman, J.C., 2001. Breaking Ostwald's rule. Chemie Der Edre-Geochemistry 61 (3), 224–235.

Dove, P., de Yoreo, J.J., 2010. Extending BCF theory through nanoscale insights: kink-limited kinetics of calcite growth and inhibition. Geochimica et Cosmochimica Acta 74 (11 (Suppl. 1)), A245.

Duan, R., Carey, J.W., Kaszuba, J.P., 2005. Mineral chemistry and precipitation kinetics of dawsonite in the geological sequestration of CO_2. American Geophysical Union, Fall Meeting 2005, abstract #GC13A-1210.

Enting, I.G., Etheridge, D.M., Fielding, M.J., 2008. A perturbation analysis of the climate benefit from geosequestration of carbon dioxide. International Journal of Greenhouse Gas Control 2, 289–296.

Fischer, C., Lüttge, A., 2007. Converged surface roughness—a new tool to quantify rock surface morphology and reactive alteration. American Journal of Science 307, 955–973.

Flaathen, T.K., Gislason, S.R., Oelkers, E.H., Sveinbjörnsdóttir, Á.E., 2009. Chemical evolution of the Mt. Hekla, Iceland, groundwaters: a natural analogue for CO_2 sequestration in basaltic rocks. Applied Geochemistry 24 (3), 463–474.

Ganor, J., Huston, T.J., Walter, L.M., 2005. Quartz precipitation kinetics at 180 °C in NaCl solutions - Implications for the usability of the principle of detailed balancing. Geochimica et Cosmochimica Acta 69 (8), 2043–2056.

Gao, Y., Liu, L., Hu, W., 2009. Petrology and isotopic geochemistry of dawsonite-bearing sandstones in Hailaer basin, northeastern China. Applied Geochemistry 24 (9), 1724–1738.

Gaus, I., Azaroual, M., Czernichowski-Lauriol, I., 2005. Reactive transport modelling of the impact of CO_2 injection on the clayey cap rock at Sleipner (North Sea). Chemical Geology 217 (3–4), 319–337.

Gaus, I., Le Guern, C., Pauwels, H., Girard, J.-P., Pearce, J., Shepherd, T., Hatziyannis, G., Metaxas, A., 2004. Comparison of long term geochemical interactions at two natural CO2-analogues: Montmiral (Southeast Basin, France) and Messokampos (Florina Basin, Greece) case studies. In: GHGT7-7th International Conference on Greenhouse Gas Control Technologies, Vancouver, Canada, September 5–9, 2004 , 9 pp.

Gaus, I., Audigane, P., André, L., Lions, J., Jacquement, N., Durst, P., Czernichowski-Lauriol, I., Azaroual, M., 2008. Geochemical and solute transport modelling for CO_2 storage, what to expect from it? International Journal of Greenhouse Gas Control 2, 605–625.

Gaus, I., 2010. Role and impact of CO_2–rock interactions during CO_2 storage in sedimentary rocks. International Journal of Greenhouse Gas Control 4, 73–89.

Gautier, J.M., Oelkers, E.H., Schott, J., 1994. Experimental-study of K-feldspar dissolution rates as a function of chemical affinity at 150 °C and pH 9. Geochimica et Cosmochimica Acta 58 (21), 4549–4560.

Gislason, S.R., Wolff-Boenisch, D., Stefanson, A., Oelkers, E.H., Gunnlaugsson, E., Sigurdardottir, H., Sigfusson, B., Broecker, W.S., Matter, J.M., Stute, M., Axelsson, G., Fridriksson, T., 2010. Mineral sequestration of carbon dioxide in basalt: a pre-injection overview of the CarbFix project. International Journal of Greenhouse Gas Control 4 (3), 537–545.

Golab, A.N., Carr, P.F., Palamara, D.R., 2006. Influence of localised igneous activity on cleat dawsonite formation in Late Permian coal measures, Upper Hunter Valley, Australia. International Journal of Coal Geology 66, 296–304.

Golab, A.N., Hutton, A.C., French, D., 2007. Petrography, carbonate mineralogy and geochemistry of thermally altered coal in Permian coal measures, Hunter Valley, Australia. International Journal of Coal Geology 70 (1–3), 150–165.

Golubev, S.V., Bauer, A., Pokrovsky, O.S., 2006. Effect of pH and organic ligands on the kinetics of smectite dissolution at 25 °C. Geochimica et Cosmochimica Acta 70 (17), 4436–4451.

Golubev, S.V., Bénézeth, P., Schott, J., Dandurand, J.L., Castillo, A., 2009. Siderite dissolution kinetics in acidic aqueous solutions from 25 to 100 °C and 0 to 50 atm pCO_2. Chemical Geology 265 (1–2), 13–19.

Gregersen, U., Johannessen, P.N., 2007. Distribution of the Neogene Utsira Sand and the succeeding deposits in the Viking Graben area, North Sea. Marine and Petroleum Geology 24 (10), 591–606.

Gregersen, U., Johannesen, P.N., Møller, J.J., Kristensen, L., Christensen, N.P., Holloway, S., Chadwick, A., Kirby, G., Lindeberg, E., Zweigel, P., 1998. Saline aquifer CO_2 storage S.A.C.S. Phase Zero 1998. Report.

Haszeldine, R.S., Quinn, O., England, G., Wilkinson, M., Shipton, Z.K., Evans, J.P., Heath, J., Crossey, L., Ballentine, C.J., Graham, C.M., 2005. Natural geochemical analogues for carbon dioxide storage in deep geological porous reservoirs, a United Kingdom perspective. Oil & Gas Science and Technology—Revue De L Institut Francais Du Petrole 60 (1), 33–49.

Hellevang, H., Aagaard, P., 2010. Can carbonate precipitation rates be derived from dissolution rate data? Geochimica et Cosmochimica Acta 74 (11 (Suppl. 1)), A396.

Hellevang, H., Kvamme, B., 2006. ACCRETE—Geochemistry solver for CO_2–water–rock interactions. In: Proceedings GHGT 8 conference.

Hellevang, H., Aagaard, P., Oelkers, E.H., Kvamme, B., 2005. Can dawsonite permanently trap CO_2? Environmental Science & Technology 39 (21), 8281–8287.

Hellevang, H., Declercq, J., Kvamme, B., Aagaard, P., 2010. The dissolution rates of dawsonite at pH 0.9 to 6.3 and temperatures of 22, 60 and 77 °C. Applied Geochemistry 25 (10), 1575–1586.

Hermanrud, C., Andresen, T., Eiken, O., Hansen, H., Janbu, A., Lippard, J., Bolås, H.N., Simmenes, T.H., Teige, G.M.G., Østmo, S., 2009. Storage of CO_2 in saline aquifers—lessons learned from 10 years of injection into the Utsira Formation in the Sleipner area. Energy Procedia 1 (1), 1997–2004.

Holloway, S., 2004. Underground sequestration of carbon dioxide—a viable greenhouse gas mitigation option. Energy 30 (11–12), 2318–2333.

IPCC, 2005. In: Metz, B., Davidson, O., Coninck, H., Loos, M., Meyer, L. (Eds.), IPCC Special Report on Carbon Dioxide Capture and Storage. Prepared by Working Group III of the Intergovernmental Panel on Climate Change. Cambridge University Press, Cambridge, United Kingdom and New York, NY, USA, 442 pp.

Johnson, J.W., Nitao, J.J., Knauss, K.G., 2004. Reactive transport modeling of CO_2 storage in saline aquifers to elucidate fundamental processes, trapping mechanisms and sequestration partitioning. In: Bains, S.J., Worden, R.H. (Eds.), Geological storage of carbon dioxide. Geological Society Special Publications, London, pp. 107–128.

Johnson, J.W., Nitao, J.J., Morris, J.P., 2005. Reactive Transport Modeling of Cap-Rock Integrity During Natural and Engineered CO_2 Storage, Carbon Dioxide Capture for Storage in Deep Geologic Formations, pp. 787–813.

Johnson, J.W., Oelkers, E.H., Helgeson, H.C., 1992. SUPCRT92: A software package for calculating the standard molal thermodynamic properties of minerals, gases, aqueous species, and reactions from 1 to 5000 bar and 0 to 1000 °C. Computers & Geosciences 18 (7), 899–947.

Ketzer, J.M., Iglesias, R., Einloft, S., Dullius, J., Ligabue, R., de Lima, V., 2009. Water–rock–CO_2 interactions in saline aquifers aimed for carbon dioxide storage: experimental and numerical modeling studies of the Rio Bonito Formation (Permian), southern Brazil. Applied Geochemistry 24 (5), 760–767.

Knauss, K.G., Johnson, J.W., Steefel, C.I., 2005. Evaluation of the impact of CO_2, co-contaminant gas, aqueous fluid and reservoir rock interactions on the geologic sequestration of CO_2. Chemical Geology 217 (3–4), 339–350.

Land, L.S., 1998. Failure to precipitate dolomite at 25 °C from dilute solution despite 1000-fold oversaturation after 32 years. Aquatic geochemistry 4, 361–368.

Lasaga, A.C., 1981. Transition state theory. In: Lasaga, A.C., Kirkpatrick, R.J. (Eds.), Kinetics of Geochemical Processes. Mineralogical Society of America, pp. 135–169.

Lasaga, A.C., 1984. Chemical-kinetics of water–rock interactions. Journal of Geophysical Research 89 (Nb6), 4009–4025.

Lu, J., Wilkinson, M., Haszeldine, R.S., Fallick, A.E., 2009. Long-term performance of a mudrock seal in natural CO_2 storage. Geology 37 (1), 35–38.

Lüttge, A., Winkler, U., Lasaga, A.C., 2003. Interferometric study of the dolomite dissolution: a new conceptual model for mineral dissolution. Geochimica et Cosmochimica Acta 67 (6), 1099–1116.

Lüttge, A., Arvidson, R., 2010. Kink site reaction kinetics: a new model unifies crystal dissolution and growth theory. Geochimica et Cosmochimica Acta 74 (11 (Suppl. 1)), A645.

Macaulay, C.I., Haszeldine, R.S., Fallick, A.E., 1993. Distribution, chemistry, isotopic composition and origin of diagenetic carbonates: Magnus sandstone, North Sea. Journal Sedimentary Petrology 63, 33–43.

Moore, J., Adams, M., Allis, R., Lutz, S., Rauzi, S., 2005. Mineralogical and geochemical consequences of the long-term presence of CO_2 in natural reservoirs: An example from the Springerville-St. Johns Field, Arizona, and New Mexico, U.S.A. Chemical Geology 217 (3–4), 365–385.

Nagy, K.L., 1995. Dissolution and precipitation kinetics of sheet silicates. In: White, A.F., Brantley, S.L. (Eds.), Chemical Weathering Rates of Silicate Minerals, vol.31. Mineralogical Society of America, Washington, DC, pp. 173–233.

Nagy, K.L., Lasaga, A.C., 1992. Dissolution and precipitation kinetics of gibbsite at 80 °C and pH 3: the dependence on solution saturation state. Geochimica et Cosmochimica Acta 56 (8), 3093–3111.

Nielsen, A.E., 1983. Precipitates: formation, coprecipitation, and aging. In: Kolthoff, I.M., Elving, P.J. (Eds.), Treatise on Analytical Chemistry. Wiley, pp. 269–347.

Oelkers, E.H., Schott, J., Gauthier, J.-M., Herrero-Roncal, T., 2008. An experimental study of the dissolution mechanism and rates of muscovite. Geochimica et Cosmochimica Acta 72 (20), 4948–4961.

Palandri, J.L., Kharaka, Y.K., 2004. A compilation of rate parameters of water–mineral interaction kinetics for application to geochemical modeling. USGS Open File Report 2004-1068, 70p.

Parkhurst, D.L., Appelo, C.A.J., 1999. User's guide to PHREEQC (version 2)—a computer program for speciation, reaction-path, 1D-transport, and inverse geochemical calculations. US Geological Survey, Water Resources Investigation Reports, pp. 312.

Pauwels, H., Gaus, I., le Nindre, Y.M., Pearce, J., Czernichowski-Lauriol, I., 2007. Chemistry of fluids from a natural analogue for a geological CO_2 storage site (Montmiral, France): lessons for CO_2–water–rock interaction assessment and monitoring. Applied Geochemistry 22 (12), 2817–2833.

Pearce, J.M., Holloway, S., Wacker, H., Nelis, M.K., Rochelle, C., Bateman, K., 1996. Natural occurences as analogues for the geological disposal of carbon dioxide. Energy Conversion and Management 37, 1123–1128.

Pokrovsky, O.S., Golubev, S.V., Schott, J., 2005. Dissolution kinetics of calcite, dolomite and magnesite at 25 °C and 0 to 50 atm pCO_2. Chemical Geology 217 (3–4), 239–255.

Pokrovsky, O.S., Golubev, S.V., Schott, J., Castillo, A., 2009. Calcite, dolomite and magnesite dissolution kinetics in aqueous solutions at acid to circumneutral pH, 25 to 150 °C and 1 to 55 atm pCO_2: new constraints on CO_2 sequestration in sedimentary basins. Chemical Geology 265 (1–2), 20–32.

Raistrick, M., Hutcheon, I., Shevalier, M., Nightingale, M., Johnson, G., Taylor, S., Mayer, B., Durocher, K., Perkins, E., Gunter, B., 2009. Carbon dioxide–water–silicate mineral reactions enhance CO_2 storage; evidence from produced fluid measurements and geochemical modeling at the IEA Weyburn-Midale Project. Energy Procedia 1 (1), 3149–3155.

Ranaweera, H.K.A., 1987. Sleipner Vest field—Norway, Southern Viking graben, North sea. In: Spencer, A.M. (Ed.), Geology of the Norwegian Oil and Gas fields, pp. 253–264.

Saldi, G.D., Jordan, G., Schott, J., Oelkers, E.H., 2009. Magnesite growth rates as a function of temperature and saturation state. Geochimica et Cosmochimica Acta 73 (19), 5646–5657.

Shiraki, R., Brantley, S.L., 1995. Kinetics of near-equilibrium calcite precipitation at 100 °C: An evaluation of elementary reaction-based and affinity-based rate laws. Geochimica et Cosmochimica Acta 59 (8), 1457–1471.

Smith, J.W., Milton, C., 1966. Dawsonite in the green river formation of Colorado. Economic Geology 61, 1029–1042.

Soave, G., 1972. Equilibrium constants from a modified Redlich–Kwong equation of state. Chemical Engineering Science 27, 1197–1203.

Steefel, C.I., Van Cappelen, P., 1990. A new kinetic approach to modeling water–rock interaction: the role of nucleation, precursors, and Ostwald ripening. Geochimica et Cosmochimica Acta 54, 2657–2677.

Tardy, Y., Duplay, J., 1994. Stability fields of smectites and illites including glauconites as a function of temperature and chemical composition. In: Wolf K.H., Chilingarian G.V. (Eds.), Diagenesis, IV. Developments in Sedimentology, vol. 51, pp. 95–132 (Chapter 5).

Tester, J.W., Worley, W.G., Robinson, B.A., Grigsby, C.O., Feerer, J.L., 1994. Correlating quartz dissolution kinetics in pure water from 25 to 625 °C. Geochimica et Cosmochimica Acta 58 (11), 2407–2420.

Teng, H.H., Dove, P.M., De Yoreo, J.J., 2000. Kinetics of calcite growth: surface processes and relationships to macroscopic rate laws. Geochimica et Cosmochimica Acta 64, 2255–2266.

Thibeau, S., Nghiem, L.X., Ohkuma, H., 2007. A modeling study of the role of selected minerals in enhancing CO_2 mineralization during CO_2 aquifer storage. In: SPE Annual Technical Conference and Exhibition, 11-14 November 2007 , Anaheim, California, U.S.A.

Verdoes, D., Kashciev, D., van Rosmalen, G.M., 1992. Determination of nucleation and growth rates from induction times in seeded and unseeded precipitation of calcium carbonate. Journal of Crystal Growth 118, 401–413.

Walton, A.G., 1967. The Formation and Properties of Precipitates. Interscience Publ, New York, 232p.

Watson, M.N., Zwingmann, N., Lemon, N.M., 2004. The Ladbroke Grove–Katnook carbon dioxide natural laboratory: a recent CO_2 accumulation in a lithic sandstone reservoir. Energy 29 (9–10), 1457–1466.

White, A.F., Peterson, M.L., Hochella Jr., M.F., 1994. Electrochemistry and dissolution kinetics of magnetite and ilmenite. Geochimica et Cosmochimica Acta 58 (8), 1859–1875.

Williamson, M.A., Rimstidt, J.D., 1994. The kinetics and electrochemical rate-determining step of aqueous pyrite oxidation. Geochimica et Cosmochimica Acta 58 (24), 5443–5454.

Woods, T.L., Garrels, R.M., 1992. Calculated aqueous-solution–solid-solution relations in the low-temperature system CaO–MgO–FeO–CO_2–H_2O. Geochimica et Cosmochimica Acta 56 (8), 3031–3043.

Worden, R.H., 2006. Dawsonite cement in the Triassic Lam Formation, Shabwa Basin, Yemen: a natural analogue for a potential mineral product of subsurface CO_2 storage for greenhouse gas reduction. Marine and Petroleum Geology 23 (1), 61–77.

Xu, T., Apps, J.A., Pruess, K., 2004. Numerical simulation of CO_2 disposal by mineral trapping in deep aquifers. Applied Geochemistry 19 (6), 917–936.

Xu, T., Apps, J.A., Pruess, K., Yamamoto, H., 2007. Numerical modeling of injection and mineral trapping Of CO_2 with H_2S and SO_2 in a sandstone formation. Chemical Geology 242 (3–4), 319–346.

Yang, L., Steefel, C.I., 2008. Kaolinite dissolution and precipitation kinetics at 22 °C and pH 4. Geochimica et Cosmochimica Acta 72 (1), 99–116.

Zerai, B., Saylor, B.Z., Matisoff, G., 2006. Computer simulation of CO_2 trapped through mineral precipitation in the Rose Run Sandstone, Ohio. Applied Geochemistry 21 (2), 223–240.

Zhang, W., Li, Y., Xu, T., Cheng, H., Zheng, Y., Xiong, P., 2009. Long-term variations of CO_2 trapped in different mechanisms in deep saline formations: a case study of the Songliao Basin, China. International Journal of Greenhouse Gas Control 3 (2), 161–180.